Mineralogical Magazine (2023), **87**, 348–355
doi:10.1180/mgm.2022.128

CAMBRIDGE UNIVERSITY PRESS

Article

Shinarumpite, a new cobalt uranyl sulfate mineral from the Scenic mine, San Juan County, Utah, USA, structurally related to leydetite

Anthony R. Kampf[1]*, Jakub Plášil[2], Travis A. Olds[3], Chi Ma[4] and Joe Marty[1]

[1]Mineral Sciences Department, Natural History Museum of Los Angeles County, 900 Exposition Boulevard, Los Angeles, CA 90007, USA; [2]Institute of Physics of the CAS, v.v.i., Na Slovance 1999/2, 18220 Prague 8, Czech Republic; [3]Section of Minerals and Earth Sciences, Carnegie Museum of Natural History, 4400 Forbes Avenue, Pittsburgh, PA 15213, USA; and [4]Division of Geological and Planetary Sciences, California Institute of Technology, Pasadena, CA 91125, USA

Abstract

The new mineral shinarumpite (IMA2021-105), $[Co(H_2O)_6][(UO_2)(SO_4)_2(H_2O)]\cdot 4H_2O$, was found in the Scenic mine on Fry Mesa, White Canyon district, San Juan County, Utah, USA, where it occurs as a secondary phase on granular quartz matrix in association with gypsum, deliensite, Co-rich rietveldite, scenicite, shumwayite and sulfur. Shinarumpite crystals are transparent, yellow, blades or prisms, up to 1 mm in length. The mineral has white streak, vitreous lustre and is nonfluorescent. It is brittle with irregular, curved fracture. The Mohs hardness is ~2½ and it has a perfect {100} cleavage. The density is 2.58(2) g·cm^{-3}. Optically, the mineral is biaxial (–) with $\alpha = 1.515(2)$, $\beta = 1.526(2)$, $\gamma = 1.529(2)$ (white light); $2V = 55(1)°$; extreme $r < v$ dispersion; orientation: $Z = \mathbf{b}$, $X \wedge \mathbf{a} = 30°$ in obtuse β; pleochroism: X = very pale yellow, Y = pale yellow, Z = light yellow; $X < Y < Z$. The Raman spectrum exhibits bands consistent with UO_2^{2+}, SO_4^{2-} and O–H. Electron microprobe analysis provided the empirical formula $[(Co_{0.51}Ni_{0.28}Fe_{0.21})_{\Sigma 1.00}(H_2O)_6][(UO_2)(SO_4)_2(H_2O)]\cdot 4H_2O$. The five strongest powder X-ray diffraction lines are [d_{obs} Å(I)(hkl)]: 10.37(100)(200), 5.73(43)(111), 5.20(70)(400, 202, 211), 4.70(31)($\bar{3}$11) and 3.326(30)(213, 021). Shinarumpite is monoclinic, $P2_1/c$, $a = 21.0549(15)$, $b = 6.8708(5)$, $c = 12.9106(5)$, $\beta = 96.678(7)°$, $V = 1885.03(17)$ Å^3 and $Z = 4$. In the structure of shinarumpite ($R_1 = 0.0336$ for 2623 $I > 2\sigma I$), linkages of pentagonal bipyramids and tetrahedra form an infinite $[(UO_2)(SO_4)_2(H_2O)]^{2-}$ sheet. Isolated $Co(H_2O)_6$ octahedra and H_2O groups occupy the interlayer region linking the sheets *via* an extensive system of hydrogen bonds. The structure of shinarumpite is very similar to that of leydetite. Uranyl sulfate structural unit types are discussed with respect to frequency and charge deficiency per anion (*CDA*).

Keywords: shinarumpite, new mineral, uranyl sulfate, crystal structure, Raman spectroscopy, leydetite, Scenic mine, White Canyon district, Utah, USA

(Received 26 June 2022; accepted 11 November 2022; Accepted Manuscript published online: 28 November 2022; Associate Editor: Michael Rumsey)

Introduction

During the last twenty years, more than 40 new uranyl sulfates have been discovered as post-mining phases on the walls of mining tunnels in inactive uranium mines, mostly in mines in the White Canyon district of south-eastern Utah, USA and at Jáchymov, Czech Republic. We now realise that the diversity of secondary minerals formed by oxidation–hydration weathering of uraninite at ambient temperatures is much greater than previously thought. This diversity can be attributed to several factors including (1) relatively low pH caused by the release of sulfuric acid from altering sulfides (principally pyrite); (2) concentrations of 'dissolved' uranium in aqueous solutions; and (3) concentrations of various cations originating both from altered primary minerals or from the surrounding country rock (Plášil *et al.*, 2022). The new mineral shinarumpite, described herein, adds to the remarkable diversity of uranyl sulfate minerals.

***Author for correspondence:** Anthony R. Kampf, Email: akampf@nhm.org
Cite this article: Kampf A.R., Plášil J., Olds T.A., Ma C. and Marty J. (2023) Shinarumpite, a new cobalt uranyl sulfate mineral from the Scenic mine, San Juan County, Utah, USA, structurally related to leydetite. *Mineralogical Magazine* **87**, 348–355. https://doi.org/10.1180/mgm.2022.128

Shinarumpite is named for the Shinarump member of the Upper Triassic Chinle formation. The uranium deposits in the White Canyon district occur within the Shinarump member. The Shinarump is the basal member of the Chinle formation. It consists primarily of sandstone, conglomerate and rare lenses of mudstone deposited by braided stream systems. The Shinarump is highly resistant to erosion and is prominently exposed over a large portion of the Colorado Plateau. It is the caprock for many of the mesas and buttes of Monument Valley. The word 'shinarump' is an old colloquial term used in the southwestern United States to refer to silicified wood; however, the Shinarump Conglomerate was first defined by G.K. Gilbert in 1875 and named for exposures in the Shinarump Cliffs, which straddle the Utah-Arizona border (Gilbert, 1875).

The new mineral and name (symbol Sru) were approved by the Commission on New Minerals, Nomenclature and Classification of the International Mineralogical Association (IMA2021-105, Kampf *et al.*, 2022a). The description is based on one holotype and three cotype specimens deposited in the collections of the Natural History Museum of Los Angeles County, 900 Exposition Boulevard, Los Angeles, CA 90007, USA, catalogue numbers 76199 (holotype), 76200, 76201 and 76202.

Occurrence

Shinarumpite was first discovered on a specimen collected by one of the authors (JM) underground in the Scenic mine (37°38'43"N, 110°07'10"W) on Fry Mesa, White Canyon district, San Juan County, Utah, USA. The uranium deposits in the White Canyon district (Chenoweth, 1993) occur within the Shinarump member of the Upper Triassic Chinle Formation, in channels incised into the reddish-brown siltstones of the underlying Lower Triassic Moenkopi Formation. The Shinarump member consists of medium- to coarse-grained sandstone, conglomeratic sandstone beds and thick siltstone lenses. Ore minerals (uraninite, montroseite, coffinite, etc.) were deposited as replacements of wood and other organic material and as disseminations in the enclosing sandstone. Since the mine closed, oxidation of primary ores in the humid underground environment has produced a variety of secondary minerals, mainly carbonates and sulfates, as efflorescent crusts on the surfaces of mine walls.

Shinarumpite is a rare mineral in the secondary mineral assemblage. It occurs on matrix comprised mostly of subhedral to euhedral, equant quartz crystals that are recrystallised counterparts of the original grains of the sandstone. It is associated with gypsum, deliensite, Co-rich rietveldite, scenicite (Kampf *et al.*, 2022b), shumwayite and sulfur. Shinarumpite alters by apparent dehydration to Co-rich rietveldite.

Physical and optical properties

Shinarumpite crystals are flattened rectangular prisms, up to ~1 mm in length, occurring in subparallel and divergent intergrowths (Fig. 1). Blades are elongated parallel to [010], flattened on {100} and exhibit the forms {100}, {010} and {001}. Crystals are yellow and transparent with vitreous lustre and white streak. The mineral is nonfluorescent. The Mohs hardness is ~2½, based upon scratch tests. Crystals are brittle with irregular, curved fracture. There is perfect cleavage on {100}. Shinarumpite is readily soluble in room-temperature H_2O. The density measured by flotation in a mixture of methylene iodide and toluene is 2.58(2) g·cm^{-3}. The calculated density is 2.569 g·cm^{-3} for the empirical formula and 2.575 g·cm^{-3} for the ideal formula.

Optically, shinarumpite is biaxial (–), with $\alpha = 1.515(2)$, $\beta = 1.526(2)$, $\gamma = 1.529(2)$ (measured in white light). The measured 2V from extinction data analysed using *EXCALIBRW* (Gunter *et al.*, 2004) is 55(1)°; the calculated 2V is 54.8°. Dispersion is $r < v$, strong. The optical orientation is $Z = \mathbf{b}$, $X \wedge \mathbf{a} = 30°$ in the obtuse angle β. The mineral is pleochroic with X = very pale yellow, Y = pale yellow, Z = light yellow; $X < Y < Z$. The Gladstone–Dale compatibility index $1 - (K_P/K_C)$ for the empirical formula is –0.024, in the excellent range (Mandarino, 2007), using $k(UO_3) = 0.118$, as provided by Mandarino (1976).

Raman spectroscopy

Raman spectroscopy was done using a Horiba XploRA PLUS using a 532 nm diode laser, a 100 μm slit, a 1800 gr/mm diffraction grating and a 100× (0.9 NA) objective. The Raman spectrum of shinarumpite from 4000 to 60 cm^{-1} is shown in Fig. 2.

A broad band consisting of several overlapping vibrations in the 3600 to 3000 cm^{-1} range (the most prominent are those at 3519, 3490, 3408, 3399 and 3330 cm^{-1}) are attributed to the ν O–H stretching vibrations of the H_2O molecules. This set of bands is comparable to that observed, for instance, for shumwayite and the synthetic phase, $UO_2SO_4{\cdot}2.5H_2O$ (Vlček *et al.*, 2009; Kampf *et al.*, 2017a). According to the correlation given by Libowitzky (1999), the approximate O–H···O hydrogen bond lengths range between 3.0 and 2.7 Å, in excellent agreement with those observed in the crystal structure (2.95–2.69 Å). In the region of the ν_2 (δ) H_2O bending vibrations, no peaks were observed, which is not unusual in Raman spectroscopy of hydrated minerals. Instead, the higher background observed there is a spectral artifact.

Fig. 1. Yellow shinarumpite prisms partially encrusted with Co-rich rietveldite on holotype specimen (#76199); field of view 0.84 mm across.

The bands at 1188, 1123 and 1102 cm^{-1} are assigned to the split triply degenerate ν_3 antisymmetric stretching vibrations of the SO_4 tetrahedra. The band at 1013 cm^{-1} and shoulder at 1001 cm^{-1} are assigned to the ν_1 symmetric stretching vibrations of structurally independent SO_4 tetrahedra. Some overlaps of these bands with the librations of H_2O are to be expected (see Colmenero *et al.*, 2020).

The Raman band at 927 cm^{-1} is attributed to the ν_3 antisymmetric stretching vibration of the uranyl ion, UO_2^{2+}. The most prominent Raman band at 839 cm^{-1} is attributed to the ν_1 symmetric stretching vibration of the uranyl ion. The inferred U–O bond-lengths (after Bartlett and Cooney, 1989) of the uranyl group, ~1.77 Å (from both ν_1 and ν_3), are within the range derived from the current X-ray study.

The bands at 658 and 602 cm^{-1} have been assigned to the ν_4 (δ) triply degenerated antisymmetric stretching vibrations of SO_4 tetrahedra. Raman bands centred at 448 and 438 cm^{-1} are related to the split ν_2 (δ) doubly degenerate bending vibrations of the SO_4 tetrahedra.

https://doi.org/10.1180/mgm.2022.128 Published online by Cambridge University Press

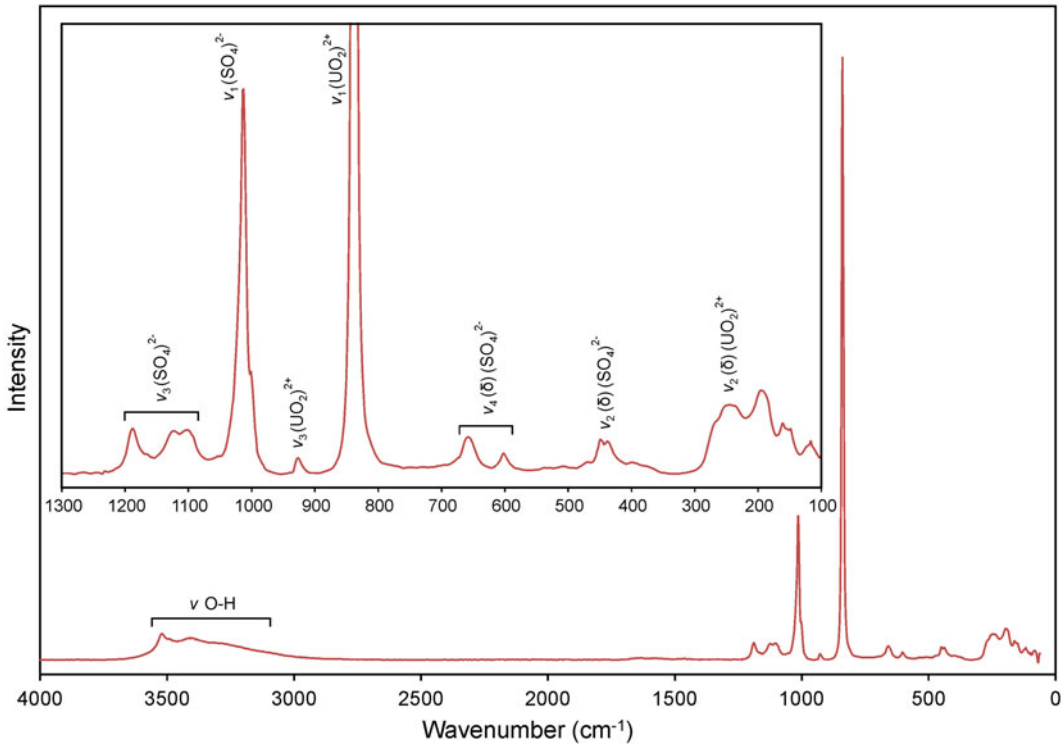

Fig. 2. Raman spectrum of shinarumpite recorded with a 532 nm laser.

The ν_2 (δ) doubly degenerate bending vibrations of UO_2^{2+} (see Kampf *et al.*, 2017a; Plášil *et al.*, 2010; Colmenero *et al.*, 2020 and others) probably contribute to the multiple bands centred at ~243 cm^{-1}, whereas Colmenero *et al.* (2020) showed that the contribution of the bending energies of the uranyl ions in the structure is distributed over a wider energy region and thus, probably the strong band at 195 cm^{-1} is also actually the result of energy overlap between ν_2 (δ) UO_2^{2+} and, for instance, U–O_{eq}–(H_2O) stretches and bends. Weak bands at the lowest energies can be assigned to unclassified lattice modes, most probably skeletal vibrations of the entire infinite sheets of polyhedra.

Chemical composition

Electron microprobe analysis (EPMA) of shinarumpite from the Scenic mine (7 points) were performed at Caltech on a JEOL 8200 electron microprobe in wavelength dispersive mode. Analytical conditions were 15 kV accelerating voltage, 10 nA beam current and 10 μm beam diameter. Insufficient material is available for CHN analysis; however, the fully ordered structure unambiguously established the quantitative content of H_2O. Analytical data are given in Table 1. The empirical formula (calculated on the basis of 21 O atoms per formula unit) is $Co_{0.51}Ni_{0.28}Fe_{0.21}U_{1.00}S_{2.00}O_{21}H_{22}$ or, arranged structurally,

Table 1. Chemical composition (in wt.%) for shinarumpite.

Constituent	Mean	Range	S.D.	Standard
FeO	2.11	1.89–2.45	0.21	fayalite
CoO	5.35	4.86–5.69	0.28	Co metal
NiO	2.92	2.56–3.30	0.22	synthetic NiO
UO_3	39.84	39.23–40.54	0.52	synthetic UO_2
SO_3	22.46	21.53–23.28	0.77	anhydrite
H_2O*	27.74			
Total	100.42			

* Based on the structure; S.D. – standard deviation.

Table 2. Data collection and structure refinement details for shinarumpite.*

Crystal data	
Structural formula	$[Co(H_2O)_6][(UO_2)(SO_4)_2(H_2O)]\cdot 4H_2O$
Space group	$P2_1/c$ (#14)
Unit cell dimensions:	
a, b, c (Å)	21.0549(15), 6.8708(3), c = 12.9106(5)
β (°)	96.678(7)
V (Å^3)	1855.03(17)
Z	4
Density (for above formula) (g·cm^{-3})	2.575
Temperature (K)	293(2)
Data collection	
Diffractometer	Rigaku R-Axis Rapid II
X-ray radiation/power	MoKα (λ = 0.71075 Å)/50 kV, 40 mA
Crystal size (μm)	100 × 70 × 20
Absorption coefficient (mm^{-1})	9.934
F(000)	1364
θ range (°)	3.12 to 25.03
Index ranges	$-25 \le h \le 25$, $-8 \le k \le 7$, $-13 \le l \le 15$
Reflections collected/unique	12335/3045; R_{int} = 0.068
Reflections with $I > 2\sigma I$	2623
Completeness to θ = 25.03°	93.1%
Refinement	
Refinement method	Full-matrix least-squares on F^2
Parameters/restraints	295 / 33
GoF	1.066
Final R indices [$I > 2\sigma(I)$]	R_1 = 0.0336, wR_2 = 0.0717
R indices (all data)	R_1 = 0.0427, wR_2 = 0.0774
Largest diff. peak/hole (e·A^{-3})	+2.12/–1.02

*$R_{int} = \Sigma|F_o^2 - F_o^2(\text{mean})|/\Sigma[F_o^2]$. GoF = $S = \{\Sigma[w(F_o^2 - F_c^2)^2]/(n-p)\}^{½}$. $R_1 = \Sigma||F_o| - |F_c||/\Sigma|F_o|$. $wR_2 = \{\Sigma[w(F_o^2 - F_c^2)^2]/\Sigma[w(F_o^2)^2]\}^{½}$; $w = 1/[\sigma^2(F_o^2) + (aP)^2 + bP]$ where a is 0.033, b is 7.44 and P is $[2F_c^2 + \text{Max}(F_o^2, 0)]/3$.

https://doi.org/10.1180/mgm.2022.128 Published online by Cambridge University Press

$[(Co_{0.51}Ni_{0.28}Fe_{0.21})_{\Sigma 1.00}(H_2O)_6][(UO_2)(SO_4)_2(H_2O)]\cdot 4H_2O$. The ideal formula is $[Co(H_2O)_6][(UO_2)(SO_4)_2(H_2O)]\cdot 4H_2O$, which requires CoO 10.42, UO_3 39.77, SO_3 22.26, H_2O 27.55, total 100 wt.%.

X-ray crystallography and structure refinement

Powder X–ray diffraction was done on an aggregate of unground crystal fragments using a Rigaku R-Axis Rapid II curved imaging plate microdiffractometer, with monochromatised Mo*Kα* radiation. A Gandolfi-like motion on the φ and ω axes was used to randomise the sample orientation and observed *d* values and intensities were derived by profile fitting using *JADE Pro* software (Materials Data, Inc.). The powder data are presented in Supplementary Table S1 (see below).

The single-crystal structure data were collected at room temperature using the same diffractometer and radiation noted above. Less than ideal crystal quality limited the data collection range to 50°2θ and contributed to somewhat low data completeness (93.1%). The Rigaku *CrystalClear* software package was used for processing structure data, including the application of an empirical multi-scan absorption correction using *ABSCOR* (Higashi, 2001). The structure was solved using the intrinsic-phasing algorithm of the *SHELXT* program (Sheldrick, 2015a). *SHELXL-2016* (Sheldrick, 2015b) was used for the refinement of the structure. All non-hydrogen atom sites were refined successfully with anisotropic displacement parameters. Difference-Fourier synthesis located all H atom positions, which were then refined with soft restraints of 0.82(3) Å on the O–H distances and 1.30(3) Å on the H–H distances and with the U_{eq} of each H atom set to 1.2 times that of the related O atom. The Co sites refined to very slightly less than full occupancy by Co; however, in the final refinement the sites were assigned full occupancy by Co, which had no effect on the *R* values. Because of the closeness in atomic numbers

Table 3. Atom coordinates and displacement parameters (Å^2) for shinarumpite.

	x/a	*y/b*	*z/c*	U_{eq}	U^{11}	U^{22}	U^{33}	U^{23}	U^{13}	U^{12}
U	0.74811(2)	0.07778(3)	0.64870(2)	0.01609(11)	0.02271(18)	0.01214(16)	0.01396(17)	0.00052(10)	0.00437(11)	0.00000(10)
Co1	0	½	0	0.0269(4)	0.0271(9)	0.0263(8)	0.0279(8)	0.0024(7)	0.0062(7)	0.0017(6)
Co2	½	½	½	0.0294(4)	0.0274(9)	0.0327(9)	0.0290(9)	−0.0039(7)	0.0074(7)	0.0010(7)
S1	0.70631(9)	0.3677(3)	0.41563(14)	0.0194(4)	0.0297(11)	0.0147(9)	0.0149(9)	−0.0011(7)	0.0070(8)	−0.0031(7)
S2	0.78793(9)	0.5755(2)	0.72239(14)	0.0196(4)	0.0261(11)	0.0139(9)	0.0198(10)	0.0016(7)	0.0071(8)	0.0016(7)
O1	0.6541(3)	0.2442(7)	0.3718(4)	0.0310(13)	0.034(3)	0.030(3)	0.031(3)	−0.012(3)	0.010(2)	−0.010(2)
O2	0.6818(3)	0.5413(7)	0.4625(4)	0.0317(13)	0.041(4)	0.024(3)	0.031(3)	−0.005(2)	0.010(3)	0.003(2)
O3	0.7502(3)	0.2626(7)	0.4948(4)	0.0273(12)	0.038(3)	0.026(3)	0.018(3)	0.004(2)	0.005(2)	−0.001(2)
O4	0.7464(3)	0.4289(7)	0.3329(4)	0.0258(13)	0.038(4)	0.017(3)	0.024(3)	0.003(2)	0.006(2)	−0.004(2)
O5	0.8373(3)	0.5780(7)	0.6530(4)	0.0300(13)	0.026(3)	0.037(3)	0.028(3)	−0.002(2)	0.011(2)	0.001(2)
O6	0.8153(3)	0.5773(8)	0.8315(4)	0.0351(14)	0.043(4)	0.045(4)	0.017(3)	−0.001(2)	0.002(3)	0.007(3)
O7	0.7451(3)	0.4031(7)	0.7018(4)	0.0269(13)	0.041(4)	0.013(3)	0.029(3)	0.000(2)	0.012(3)	−0.002(2)
O8	0.7442(2)	0.7464(7)	0.7021(4)	0.0250(12)	0.033(3)	0.015(3)	0.029(3)	0.002(2)	0.011(2)	0.003(2)
O9	0.6639(3)	0.0741(7)	0.6299(4)	0.0251(12)	0.033(3)	0.023(3)	0.019(3)	0.004(2)	0.003(2)	0.001(2)
O10	0.8331(3)	0.0786(6)	0.6681(4)	0.0226(12)	0.034(3)	0.014(3)	0.021(3)	0.001(2)	0.004(2)	−0.001(2)
OW11	0.7511(3)	0.8690(8)	0.4997(4)	0.0362(15)	0.071(5)	0.022(3)	0.019(3)	−0.007(3)	0.020(3)	−0.013(3)
H11A	0.730(4)	0.772(9)	0.488(6)	0.043						
H11B	0.770(4)	0.888(11)	0.449(5)	0.043						
OW12	0.9734(3)	0.7548(8)	0.9245(5)	0.0441(16)	0.042(4)	0.033(4)	0.061(4)	0.022(3)	0.020(3)	0.013(3)
H12A	0.941(3)	0.821(11)	0.930(7)	0.053						
H12B	0.995(3)	0.832(10)	0.893(7)	0.053						
OW13	0.9168(3)	0.3702(9)	0.9303(6)	0.0437(16)	0.032(4)	0.035(4)	0.062(4)	0.006(3)	−0.007(3)	−0.002(3)
H13A	0.888(3)	0.424(10)	0.894(7)	0.052						
H13B	0.904(4)	0.264(7)	0.944(7)	0.052						
OW14	0.9543(3)	0.5868(8)	0.1302(5)	0.0372(15)	0.034(4)	0.035(4)	0.046(4)	−0.004(3)	0.019(3)	−0.004(3)
H14A	0.919(2)	0.551(10)	0.144(7)	0.045						
H14B	0.955(4)	0.704(5)	0.142(7)	0.045						
OW15	0.5861(3)	0.5387(12)	0.5910(5)	0.0562(19)	0.031(4)	0.096(6)	0.042(4)	−0.021(4)	0.004(3)	−0.004(4)
H15A	0.619(3)	0.524(16)	0.565(6)	0.067						
H15B	0.594(4)	0.556(15)	0.652(3)	0.067						
OW16	0.5349(3)	0.2378(9)	0.4487(5)	0.0445(16)	0.036(4)	0.040(4)	0.060(4)	−0.016(3)	0.013(3)	−0.005(3)
H16A	0.570(2)	0.254(13)	0.433(7)	0.053						
H16B	0.516(3)	0.168(12)	0.402(5)	0.053						
OW17	0.5367(3)	0.6479(9)	0.3760(5)	0.0427(16)	0.041(4)	0.043(4)	0.047(4)	0.002(3)	0.018(3)	−0.001(3)
H17A	0.5737(17)	0.682(12)	0.372(7)	0.051						
H17B	0.515(3)	0.747(8)	0.365(8)	0.051						
OW18	0.6290(3)	0.6289(9)	0.7945(5)	0.0377(15)	0.035(4)	0.033(3)	0.047(4)	0.011(3)	0.012(3)	0.006(3)
H18A	0.639(4)	0.519(6)	0.812(7)	0.045						
H18B	0.662(3)	0.679(10)	0.779(7)	0.045						
OW19	0.8716(3)	0.9911(10)	0.9529(5)	0.0373(14)	0.030(4)	0.048(4)	0.034(3)	−0.004(3)	0.004(3)	0.003(3)
H19A	0.839(3)	0.963(13)	0.916(5)	0.045						
H19B	0.861(4)	0.986(14)	1.012(3)	0.045						
OW20	0.9646(3)	0.5230(10)	0.6851(5)	0.0400(15)	0.033(4)	0.048(4)	0.039(4)	0.005(3)	0.004(3)	0.011(3)
H20A	0.9258(15)	0.532(14)	0.689(6)	0.048						
H20B	0.980(3)	0.506(15)	0.746(3)	0.048						
OW21	0.4655(3)	0.9655(10)	0.3218(5)	0.0434(16)	0.035(4)	0.053(4)	0.043(4)	0.008(3)	0.010(3)	−0.008(3)
H21A	0.4278(19)	0.969(14)	0.330(6)	0.052						
H21B	0.466(4)	1.000(15)	0.261(3)	0.052						

https://doi.org/10.1180/mgm.2022.128 Published online by Cambridge University Press

Table 4. Selected bond distances (Å) and angles (°) for shinarumpite.

Bond	Distance	Bond	Distance	Hydrogen bonds *D*–H···*A*	*D*–H	H···*A*	*D*···*A*	<*DHA*
Co1–OW12 ×2	2.050(5)	S1–O1	1.449(5)	OW11–H11A···O2	0.81(3)	1.88(3)	2.696(8)	179(10)
Co1–OW13 ×2	2.075(6)	S1–O2	1.460(5)	OW11–H11B···O6	0.81(3)	1.90(3)	2.713(8)	178(9)
Co1–OW14 ×2	2.118(6)	S1–O3	1.483(5)	OW12–H12A···OW19	0.83(3)	1.92(3)	2.749(9)	174(10)
<Co1–O>	2.081	S1–O4	1.497(5)	OW12–H12B···OW20	0.84(3)	1.91(3)	2.744(9)	174(8)
		<S1–O>	1.472	OW13–H13A···O6	0.81(3)	1.95(3)	2.754(8)	170(10)
Co2–OW15 ×2	2.059(7)			OW13–H13B···OW19	0.81(3)	2.00(3)	2.800(9)	170(10)
Co2–OW16 ×2	2.082(6)	S2–O5	1.449(6)	OW14–H14A···O10	0.82(3)	2.08(3)	2.888(8)	171(7)
Co2–OW17 ×2	2.117(6)	S2–O6	1.459(6)	OW14–H14B···OW20	0.82(3)	1.96(3)	2.775(9)	173(9)
<Co2–O>	2.086	S2–O7	1.494(5)	OW15–H15A···O2	0.81(3)	1.98(4)	2.754(9)	160(10)
		S2–O8	1.496(5)	OW15–H15B···OW18	0.80(3)	1.96(4)	2.748(9)	169(10)
U–O9	1.762(5)	<S2–O>	1.475	OW16–H16A···O1	0.80(3)	2.02(4)	2.805(8)	167(8)
U–O10	1.777(5)			OW16–H16B···OW21	0.83(3)	1.98(4)	2.786(9)	166(9)
U–O7	2.341(5)			OW17–H17A···OW18	0.82(3)	2.08(6)	2.776(8)	143(8)
U–O3	2.363(5)			OW17–H17B···OW21	0.82(3)	1.87(3)	2.694(9)	173(10)
U–O8	2.383(5)			OW18–H18A···O1	0.81(3)	1.98(3)	2.780(8)	172(9)
U–O4	2.383(5)			OW18–H18B···O8	0.82(3)	2.14(4)	2.939(8)	163(9)
U–OW11	2.406(5)			OW19–H19A···O4	0.81(3)	2.24(6)	2.949(8)	146(9)
<U–O_{ap}>	1.770			OW19–H19B···O5	0.82(3)	1.99(3)	2.803(8)	170(9)
<U–O_{eq}>	2.375			OW20–H20A···O5	0.83(3)	1.89(3)	2.691(8)	162(8)
				OW20–H20B···OW14	0.82(3)	2.09(4)	2.867(9)	159(8)
				OW21–H21A···O9	0.81(3)	2.09(3)	2.878(8)	168(9)
				OW21–H21B···OW17	0.83(3)	2.03(4)	2.840(9)	166(10)

D = donor; *A* = acceptor

(and scattering powers) of Fe(26), Co(27) and Ni(28), we consider the EPMA to be the best indication of the amounts of these elements present in shinarumpite, including the crystal used in the structure determination; consequently, for calculation of the bond-valences associated with the Co sites, we used the proportions of Co, Ni and Fe provided by EPMA. Data collection and refinement details are given in Table 2, atom coordinates and displacement parameters in Table 3, selected bond distances in Table 4, and a bond valence analysis in Table 5. The crystallographic information file has been deposited with the Principal Editor of *Mineralogical Magazine* and is available with the Supplementary material (see below).

Table 5. Bond valence analysis for shinarumpite. Values are expressed in valence units.

						Hydrogen bonds		
	Co1	Co2	U1	S1	S2	donated	accepted	Sum
O1				1.59			0.18, 0.19	1.96
O2				1.55			0.23, 0.20	1.98
O3			0.51	1.46				1.97
O4			0.49	1.41			0.14	2.04
O5					1.59		0.18, 0.23	2.01
O6					1.55		0.22, 0.20	1.97
O7			0.54		1.42			1.96
O8			0.49		1.41		0.14	2.04
O9			1.82				0.16	1.98
O10			1.77				0.16	1.92
OW11			0.47			−0.23, −0.22		0.02
OW12	$0.39^{\times 2\downarrow}$					−0.20, −0.21	0.13	0.11
OW13	$0.36^{\times 2\downarrow}$					−0.20, −0.18		−0.02
OW14	$0.32^{\times 2\downarrow}$					−0.16, −0.19	0.16	0.13
OW15		$0.38^{\times 2\downarrow}$				−0.20, −0.20		−0.03
OW16		$0.36^{\times 2\downarrow}$				−0.18, −0.19		−0.02
OW17		$0.32^{\times 2\downarrow}$				−0.19, −0.23	0.17	0.07
OW18						−0.19, −0.14	0.20, 0.19	0.06
OW19						−0.14, −0.18	0.20, 0.18	0.06
OW20						−0.23, −0.16	0.21, 0.19	0.01
OW21						−0.16, −0.17	0.19, 0.23	0.09
Sum	2.14	2.12	6.09	6.01	5.97			

Bond valence parameters from Gagné and Hawthorne (2015). The values for the Co sites are based on the proportions of Co, Ni and Fe provided by EPMA. Hydrogen-bond strengths are based on O–O bond lengths from Ferraris and Ivaldi (1988).

Description of the structure

The single independent U site in the structure is surrounded by seven O atoms forming a UO_7 pentagonal bipyramid. This is the most typical coordination for U^{6+}, particularly in uranyl sulfates, where the two short apical bonds of the bipyramid constitute the uranyl group. Four of the five equatorial O sites of the UO_7 bipyramid participate in two different SO_4 tetrahedra (centred by S1 and S2); the other equatorial O site is an H_2O group. The linkages of pentagonal bipyramids and tetrahedra form an infinite $[(UO_2)(SO_4)_2(H_2O)]^{2-}$ sheet in the {100} plane (Fig. 3).

Two independent Co sites (Co1 and Co2) are located on special positions (0 ½ 0) and (½ ½ ½), respectively and each is octahedrally coordinated by H_2O groups. These $Co(H_2O)_6$ octahedra, along with four isolated H_2O groups (OW18, OW19, OW20 and OW21), constitute the $[Co(H_2O)_6{\cdot}4(H_2O)]^{2+}$ interstitial complex, which links the $[(UO_2)(SO_4)_2(H_2O)]^{2-}$ sheets to one another *via* an extensive system of hydrogen bonds (Fig. 4).

The structure of shinarumpite is very similar to that of leydetite, $[Fe^{2+}(H_2O)_6][(UO_2)(SO_4)_2(H_2O)]{\cdot}4H_2O$ (Plášil *et al.*, 2013; Fig. 4). The most noteworthy structural difference is in the configurations of the $[(UO_2)(SO_4)_2(H_2O)]^{2-}$ structural units (Fig. 3). The sheet in shinarumpite is topologically identical to that in wetherillite, $[Na(H_2O)_3]_2[Mg(H_2O)_6][(UO_2)(SO_4)_2(H_2O)]_2{\cdot}4H_2O$ (Kampf *et al.*, 2015).

Discussion

Plášil *et al.* (2022) recently discussed the relationships between structure, chemical composition and occurrence for the uranyl sulfate minerals. Herein, we will expand upon that discussion

https://doi.org/10.1180/mgm.2022.128 Published online by Cambridge University Press

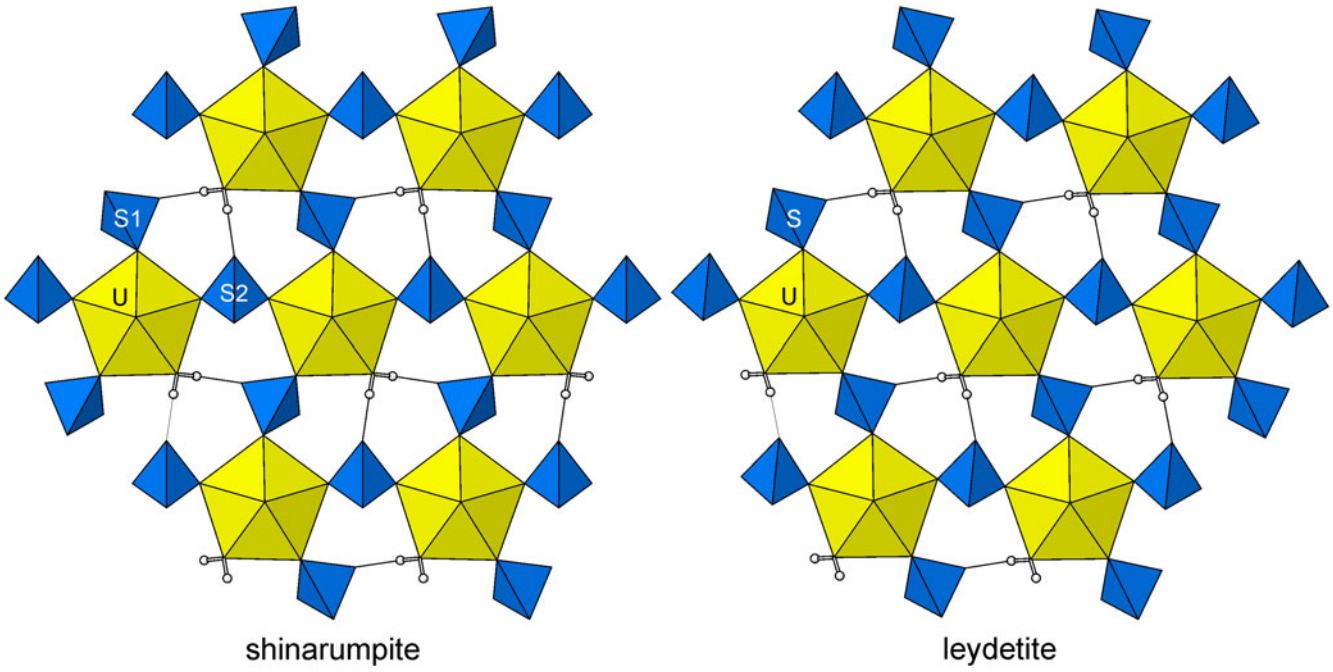

Fig. 3. The uranyl sulfate sheets of formula $[(UO_2)(SO_4)_2(H_2O)]^{2-}$ parallel to {100} in shinarumpite and parallel to {001} in leydetite. The H atoms of the H_2O groups are shown as small white balls. The hydrogen bonds are shown with thin black lines.

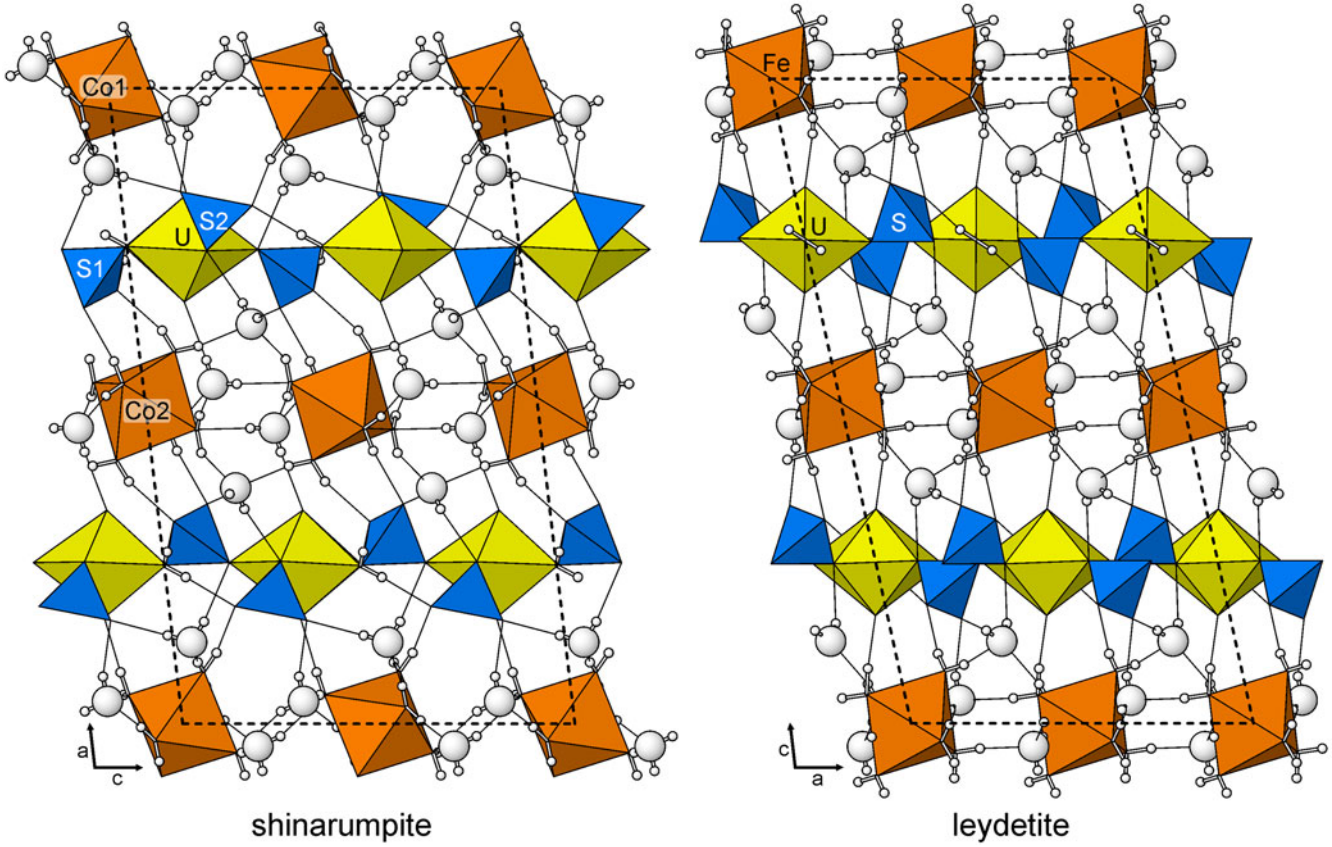

Fig. 4. The structures of shinarumpite and leydetite viewed down [010]. The O atoms of the isolated H_2O groups are shown as large white balls. The H atoms of the H_2O groups are shown as small white balls. The hydrogen bonds are shown with thin black lines. The unit-cell outlines are shown with dashed lines.

https://doi.org/10.1180/mgm.2022.128 Published online by Cambridge University Press

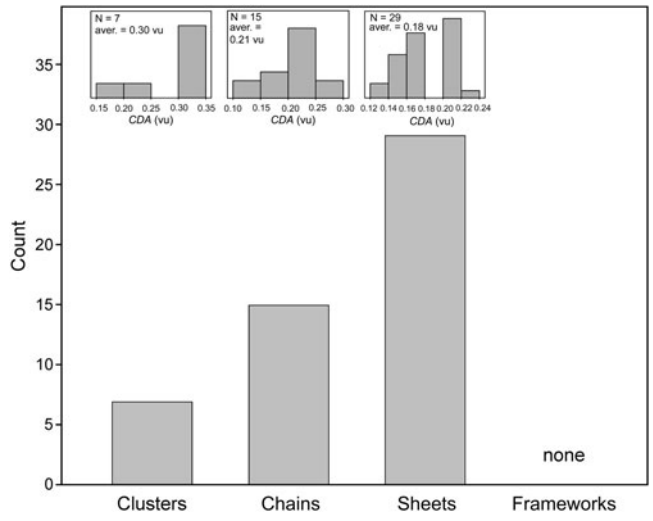

Fig. 5. The total numbers of known uranyl sulfate minerals with cluster, chain, sheet and framework structural units. Each class is further characterised by the value of the charge deficiency per anion (*CDA*) (*N* = number of uranyl sulfates in the class; aver. = average value of the *CDA*). The minerals metauranopilite (Nováček, 1935) and jáchymovite (Čejka *et al.*, 1996) are not included due to the lack of structure information.

by considering the structural typologies of known uranyl sulfate minerals as they relate to the structure hierarchy hypothesis (see Hawthorne, 2014). Figure 5 compares the numbers of uranyl sulfate minerals with structures containing cluster, chain, sheet and framework structural units constructed from linkages of uranyl bipyramids and sulfate tetrahedra. Sheet structural units are by far the most common and it is worth noting that this is also true for synthetic uranyl sulfates and even for U^{6+} phases not containing sulfate groups (see Lussier *et al.*, 2016). Interestingly, the average charge deficiency per anion (*CDA*; see Schindler and Hawthorne, 2008 and references therein) is very similar for the chains and sheets at ~0.2 valence units (vu). However, the full range in *CDA* is slightly narrower for sheets, which might reflect the somewhat greater rigidity of the sheet-like structural units in adopting possible OH/H_2O configurations. The average *CDA* value for cluster structural units is much higher, 0.3 vu, which is not very common among uranyl minerals (see Schindler and Hawthorne, 2008). It is very likely that such a high *CDA* is due to more alkaline conditions under which these minerals form, despite a much higher proportion of SO_4 within the structural units (see Plášil *et al.*, 2022). We should not forget that the activity of alkalis (manifested by a high proportion of Na and K in the structures of these cluster-based uranyl sulfates; see Plášil *et al.*, 2022) is due to, or is causing, relatively alkaline conditions. The relationship between the average Lewis basicity (or *CDA*) of the structural units and the pH of the corresponding parental solution has been provided by Schindler and Hawthorne (2001) for borate minerals. It is noteworthy that borate minerals also have relatively high *CDA* values, often exceeding 0.3 vu.

The lack of framework structures based on linkages of uranyl bipyramids and sulfate tetrahedra is not surprising, as framework structures are rare for U^{6+} minerals in general (see Lussier *et al.*, 2016). Although there are no uranyl sulfate framework structures, frameworks involving SeO_4 or MoO_4 polyhedra are known (Lussier *et al.*, 2016) and provide a rich avenue for synthetic studies. It is also worth considering the possibility of a uranyl-sulfate-based nanocluster, either in a mineral or synthetic structure. The only known naturally occurring uranyl-nanocluster mineral ewingite, $Mg_8Ca_8(UO_2)_{24}(CO_3)_{30}O_4(OH)_{12}(H_2O)_{138}$ (Olds *et al.*, 2017), contains a characteristic fundamental building unit (FBU), a pentagonal uranyl bipyramid trimer. This seems to be an important piece of the uranyl-nanocluster puzzle in natural minerals, particularly without utilising uranyl-peroxide bridges that provide effective curvature for their formation (see Burns and Nyman, 2018). Moreover, as yet, there is no evidence that peroxide-based uranyl nanoclusters are abundant in Nature. At least one known uranyl sulfate contains such an FBU. It is the mineral alwilkinsite-(Y), $Y(H_2O)_7[(UO_2)_3(SO_4)_2O(OH)_3]\cdot 7H_2O$ (Kampf *et al.*, 2017b), which contains a $[(UO_2)_3O_5(OH)_5]^{9-}$ trimer. The *CDA* of alwilkinsite-(Y), 0.18 vu, is close to the average *CDA* value for both chain and sheet uranyl sulfate structures. This suggests that some potential exists for uranyl sulfates to form exotic or novel structures based on trimers of uranyl pentagonal bipyramids. In particular, mineral associations that include zippeite-group minerals, mathesiusite, seaborgite and others having similar *CDA* values (see Plášil *et al.*, 2022) may provide opportunistic hunting grounds for new species.

Acknowledgements. Reviewer Fabrice Dal Bo and an anonymous reviewer are thanked for their helpful comments on the manuscript. A portion of this study was funded by the John Jago Trelawney Endowment to the Mineral Sciences Department of the Natural History Museum of Los Angeles County. This research was also financially supported by the Czech Science Foundation (project 20-11949S to JP).

Supplementary material. To view supplementary material for this article, please visit https://doi.org/10.1180/mgm.2022.128

Competing interests. The authors declare none.

References

Bartlett J.R., Cooney R.P. (1989) On the determination of uranium-oxygen bond lengths in dioxouranium(VI) compounds by Raman spectroscopy. *Journal of Molecular Structure*, **193**, 295–300.

Burns P.C. and Nyman M. (2018) Captivation with encapsulation: a dozen years of exploring uranyl peroxide capsules. *Dalton Transactions*, **47**, 5916–5927.

Čejka J., Sejkora J., Mrázek Z., Urbanec Z. and Jarchovský T. (1996): Jáchymovite, $(UO_2)_8(SO_4)(OH)_{14}\cdot 13H_2O$, a new uranyl mineral from Jáchymov, the Krušné Hory Mts., Czech Republic, and its comparison with uranopilite. *Neues Jahrbuch für Mineralogie Abhandlungen*, **170**, 155–170.

Chenoweth W.L. (1993) The Geology and Production History of the Uranium Deposits in the White Canyon Mining District, San Juan County, Utah. *Utah Geological Survey Miscellaneous Publication*, **93-3**.

Colmenero F., Plášil J., Němec I. (2020) Uranosphaerite: Crystal structure, hydrogen bonding, mechanics, infrared and Raman spectroscopy and thermodynamics. *Journal of Physics and Chemistry of Solids*, **141**, 109400.

Ferraris G. and Ivaldi G. (1988) Bond valence vs bond length in O···O hydrogen bonds. *Acta Crystallographica Section*, **B44**, 341–344.

Gagné O.C. and Hawthorne F.C (2015) Comprehensive derivation of bond-valence parameters for ion pairs involving oxygen. *Acta Crystallographica*, **B71**, 562–578.

Gilbert G.K. (1875) Report upon the geology of portions of Nevada, Utah, California, and Arizona, examined in the years 1871 and 1872. Pp. 17–187 in: *Report on the Geographical and Geological Explorations and Surveys West of the One Hundredth Meridian* (*Wheeler*). U.S. Geological and Geographical Survey, Publication of the Wheeler Survey, **Volume 3**.

Gunter M.E., Bandli B.R., Bloss F.D., Evans S.H., Su S.C., and Weaver R. (2004) Results from a McCrone spindle stage short course, a new version of EXCALIBR, and how to build a spindle stage. *The Microscope*, **52**, 23–39.

Hawthorne F.C. (2014) The structure hierarchy hypothesis. *Mineralogical Magazine*, **78**, 957–1027.

Higashi T. (2001) *ABSCOR*. Rigaku Corporation, Tokyo.

Kampf A.R., Plášil J., Kasatkin A.V. and Marty J. (2015) Bobcookite, NaAl$(UO_2)_2(SO_4)_4{\cdot}18H_2O$, and wetherillite, $Na_2Mg(UO_2)_2(SO_4)_4{\cdot}18H_2O$, two new uranyl sulfate minerals from the Blue Lizard mine, San Juan County, Utah, USA. *Mineralogical Magazine*, **79**, 695–714.

Kampf A.R., Plášil J., Kasatkin A.V., Marty J. Čejka J. and Ladislav Lapčák (2017a) Shumwayite, $[(UO_2)(SO_4)(H_2O)_2]_2{\cdot}H_2O$, a new uranyl sulfate mineral from Red Canyon, San Juan County, Utah, USA. *Mineralogical Magazine*, **81**, 273–285.

Kampf A.R., Plášil J., Čejka J., Marty J., Škoda R. and Lapčák L. (2017b) Alwilkinsite-(Y), a new rare-earth uranyl sulfate mineral from the Blue Lizard mine, San Juan County, Utah, USA. *Mineralogical Magazine*, **81**, 895–907.

Kampf A.R., Plášil J., Olds T.A., Ma C. and Marty J. (2022a) Shinarumpite, IMA 2021-105. CNMNC Newsletter 66. *Mineralogical Magazine*, **86**, https://doi.org/10.1180/mgm.2022.33

Kampf A.R., Plášil J., Olds T.A., Ma C. and Marty J. (2022b) Scenicite, a new uranyl-sulfate mineral from the White Canyon district, San Juan County, Utah, USA. *Mineralogical Magazine*, **86**, 743–748, https://doi.org/10.1180/mgm.2022.53

Libowitzky E. (1999) Correlation of O–H stretching frequencies and O–H···O hydrogen bond lengths in minerals. *Monatshefte für Chemie*, **130**, 1047–1059.

Lussier A.J., Lopez R.A. and Burns P.C. (2016) A revised and expanded structure hierarchy of natural and synthetic hexavalent uranium compounds. *The Canadian Mineralogist*, **54**, 177–283.

Mandarino J.A. (1976) The Gladstone-Dale relationship – Part 1: derivation of new constants. *The Canadian Mineralogist*, **14**, 498–502.

Mandarino J.A. (2007) The Gladstone–Dale compatibility of minerals and its use in selecting mineral species for further study. *The Canadian Mineralogist*, **45**, 1307–1324.

Nováček R. (1935) Study of some secondary uranium minerals. *Věstník Královské České Společnosti Nauk*, **7**, 1–16.

Olds T.A., Plášil J., Kampf A.R., Simonetti A., Sadergaski L.R., Chen Y.-S. and Burns P.C. (2017) Ewingite: Earth's most complex mineral. *Journal of Geology*, **45**, 1007–1010.

Plášil J., Buixaderas E., Čejka J., Sejkora J., Jehlička J. and Novák M. (2010) Raman spectroscopic study of the uranyl sulphate mineral zippeite: low wavenumber and U–O stretching regions. *Analytical and Bioanalytical Chemistry*, **397**, 2703–2715.

Plášil J., Kasatkin A.V., Škoda R., Novák M., Kallistová A., Dušek M., Skála R., Fejfarová K., Čejka J., Meisser N., Goethals H., Machovič V. and Lapčák. L. (2013) Leydetite, $Fe(UO_2)(SO_4)_2(H_2O)_{11}$, a new uranyl sulfate mineral from Mas d'Alary, Lodève, France. *Mineralogical Magazine*, **77**, 429–441.

Plášil J., Kampf A.R., Ma Ch. and Desor J. (2022) Oldsite, $K_2Fe^{2+}[(UO_2)(SO_4)_2]_2(H_2O)_8$, a new uranyl sulfate mineral from Utah, USA: its description and implications to the formation and occurrences of uranyl sulfate minerals. *Mineralogical Magazine*, https://doi.org/10.1180/mgm.2022.106

Schindler M. and Hawthorne F.C. (2001) A bond-valence approach to the structure, chemistry, and paragenesis of hydroxyl-hydrated oxysalt minerals. I. Theory. *The Canadian Mineralogist*, **39**, 1225–1242.

Schindler M. and Hawthorne F.C. (2008) The stereochemistry and chemical composition of interstitial complexes in uranyl-oxysalt minerals. *The Canadian Mineralogist*, **46**, 467–501.

Sheldrick G.M. (2015a) *SHELXT* – Integrated space-group and crystal-structure determination. *Acta Crystallographica*, **A71**, 3–8.

Sheldrick G.M. (2015b) Crystal structure refinement with *SHELXL*. *Acta Crystallographica*, **C71**, 3–8.

Vlček V., Čejka J., Císařová I., Goliáš V. and Plášil J. (2009) Crystal structure of $UO_2SO_4{\cdot}2.5H_2O$: Full anisotropic refinement and vibration characterization. *Journal of Molecular Structure*, **936**, 75–79.

https://doi.org/10.1180/mgm.2022.128 Published online by Cambridge University Press